Methods in Oceanography 7 (2013) 95–109

Contents lists available at ScienceDirect

Methods in Oceanography

journal homepage: www.elsevier.com/locate/mio

Full length article

The effect of suspended particle composition on particle area-to-mass ratios in coastal waters

Paul S. Hill [a,*], David G. Bowers [b], Katherine M. Braithwaite [b]

[a] *Department of Oceanography, Dalhousie University, P.O. Box 15000, Halifax, Nova Scotia, B3H 4R2, Canada*

[b] *School of Ocean Sciences, Bangor University, Menai Bridge, Anglesey LL595AB, UK*

HIGHLIGHTS

- The hypothesis that the area-to-mass ratio of organic mass is twice that of mineral mass is tested.
- The hypothesis could not be rejected.
- Particle composition may not correlate with particle size or packing geometry within aggregates.

ARTICLE INFO

Article history:
Available online 12 March 2014

Keywords:
Scattering
Attenuation
Sediment
Aggregation
LISST

ABSTRACT

Measurements of particle area, organic suspended mass, and mineral suspended mass were collected at 9 sites on the west and south coasts of Great Britain. Multiple linear regression of particle area on organic suspended mass and mineral suspended mass was used to estimate the area-to-mass ratios of organic and mineral matter. Statistically, the null hypothesis that the organic area-to-mass ratio was 2 times the mineral ratio could not be rejected. Failure to reject this hypothesis may indicate that component particle composition is not correlated with the packing geometry of aggregated particles or the size of component particles that comprise the aggregates. Alternatively, correlations between particle parameters may exist, but they offset one another, thereby producing an organic area-to-mass ratio that is not significantly different from two times the mineral area-to-mass ratio.

* Corresponding author. Tel.: +1 9024942266.
E-mail address: paul.hill@dal.ca (P.S. Hill).

http://dx.doi.org/10.1016/j.mio.2014.02.003
2211-1220/

Introduction

The application of optical sensors to the characterization of marine particle suspensions was advanced fundamentally in the late 1960s when it was demonstrated that scattering and attenuation of light are linearly correlated to the total suspended particle projected area (Beardsley et al., 1970). As a result, to a first approximation, scattering and attenuation of light in particle suspensions can be converted into particle volume or mass concentration, because volume and mass concentrations are linearly related to area concentration (Pak and Zaneveld, 1977). On the basis of this argument, optical instruments were used in the 1970s and 1980s to investigate particle processes in diverse environments, including, among others, shelf benthic nepheloid layers (Pak and Zaneveld, 1977), open-ocean basins (Plank et al., 1973), various ocean fronts (Zaneveld and Pak, 1979), shelf and slope internal nepheloid layers (Pak et al., 1980), coastal bays (Kitchen et al., 1982), nepheloid layers on the continental rise (Spinrad et al., 1983), and in river plumes (Pak et al., 1984).

Estimates of particle concentration from these various pioneering studies were attended by the caveat that the conversion from optical to particle properties depended on size, shape, structure and refractive index of particles, which were known to vary (e.g., Kitchen et al., 1982). Despite this concern, reasonable relationships between suspended particle volume and optical attenuation continued to emerge (Spinrad et al., 1983), a result that captured the attention of sedimentologists seeking automated, in situ methods for estimating suspended sediment mass concentration (e.g., Baker and Lavelle, 1984). The problem posed by variable conversion coefficients from optical properties to sediment mass, however, remained. The search for sources of variability in conversion coefficients is the topic of this manuscript.

The coefficients required to convert scattering or attenuation coefficients into mass concentration vary over an order of magnitude (Baker and Lavelle, 1984; Bowers et al., 2009; Hill et al., 2011), compromising the accuracy of optical scattering and attenuation sensors for estimating sediment mass concentration. The conversion coefficients vary because the projected-area-to-mass ratios of suspended particles vary. Baker and Lavelle (1984) showed quantitatively that the projected-area-to-mass ratio for solid spheres varies as the inverse of the product of particle density and diameter. Because particle size is variable in marine waters, size has long been suspected of causing the majority of variability in the area-to-mass ratio of particles (Baker and Lavelle, 1984; Wiberg et al., 1994; Fugate and Friedrichs, 2002; Downing, 2006). Recent work has shown, however, that size only accounts for a small fraction of the observed variability in the conversion from optical attenuation or scattering to suspended mass (Bowers et al., 2009; Hill et al., 2011; Neukermans et al., 2012). The explanation is that suspended solids are in aggregates for which particle mass varies approximately with particle area, which is linearly correlated with optical attenuation and scattering cross sections for particles that are large relative to the wavelength of light (Bowers et al., 2009; Hill et al., 2011; Neukermans et al., 2012; Boss et al., 2009; Slade et al., 2011).

Increasingly, attention is being focused on the effect of particle density on the projected-area-to-mass ratio of suspended particles (Bowers et al., 2009; Neukermans et al., 2012; Babin et al., 2003; Braithwaite et al., 2010). Aggregate density depends primarily on three parameters: component particle density, component particle size and aggregate packing geometry (Khelifa and Hill, 2006; Maggi, 2007, 2013). Component particle density depends on the composition of component particles, with mineral particles having densities that are generally twice as large as organic particle densities (cf. Babin et al., 2003). Presently, the extent to which component particle composition is correlated with component particle size and aggregate packing geometry is not known. Aggregate packing geometry is estimated from observations of particle size and settling velocity (Khelifa and Hill, 2006; Maggi, 2007, 2013), but because of the difficulty in collecting individual aggregates, most studies of this sort do not measure either component particle size or composition. The lack of direct data necessitates the use of indirect methods for exploring the extent of correlation between component particle composition, component particle size, and aggregate geometry.

Maggi (2013) explored possible correlations in the three particle parameters by dividing published size-settling velocity data into different compositional groups and then fitting the data to a model that estimated aggregate packing geometry, component particle size and component particle density. His

analysis indicated that mineral-rich aggregates have larger component particles and are less densely packed than organic-rich aggregates.

The goal of this paper is to use an alternative indirect method for exploring possible correlations between component-particle composition and component-particle size or aggregate packing geometry. Multiple linear regression of projected particle area on organic and mineral suspended mass concentration is used to estimate and compare particle projected-area-to-mass ratios for organic and inorganic matter in suspension. The comparison of the relative magnitudes of the area-to-mass ratios is used to examine whether there is evidence for systematic correlation between component particle composition and component particle size and/or aggregate packing geometry.

Theory

Particles are aggregated in the ocean, and optical properties in a wide range of environments are determined by particle aggregates more so than by single grains (see Burd and Jackson, 2009; Stemmann and Boss, 2012, for reviews). Because aggregates incorporate progressively more void spaces into their internal structure as they grow, the density of aggregates decreases with increasing size (Khelifa and Hill, 2006; Maggi, 2007, 2013), which also means that the area-to-mass ratios for aggregates are different from those of solid spheres.

Aggregates have been characterized as fractal objects, for which mass goes as diameter raised to a power less than 3 (Orbach, 1986; Logan and Wilkinson, 1990), according to an expression like

$$M = M_c \left(\frac{D}{D_c} \right)^{D3}. \tag{1}$$

In Eq. (1), M (kg) is the mass of an aggregate of diameter, D (m), and M_c (kg) is the mass of the component particles of diameter, D_c (m), that constitute the aggregate (see Table 1 for all notation). The exponent $D3$ (dimensionless) is the 3-D fractal dimension. The strict notion that a single fractal dimension characterizes the entire particle size distribution has been relaxed recently in favor of models in which the fractal dimension is replaced by an exponent that increases with decreasing size (Khelifa and Hill, 2006; Maggi, 2007, 2013). These more accurate descriptions of aggregates are necessarily more complex, so it is convenient to use the simpler expression (Eq. (1)) to explore the effects of aggregate composition and geometry on aggregate area-to-mass ratios. Similarly, particle size distributions in the ocean often are described with an overly simplified power law of the form (e.g., Stemmann and Boss, 2012):

$$n(D) = n_c \left(\frac{D}{D_c} \right)^{-b}, \tag{2}$$

where $n(D)(\mathrm{m}^{-4})$ is the number concentration of particles of diameter, D, over the interval D to $D+dD$, and $n_c(\mathrm{m}^{-4})$ is the number concentration of particles between diameters D_c and $D_c + dD$. The use of Eq. (2) to describe the size distribution also helps to illustrate the parameters that affect area-to-mass ratios.

Under the assumption that particles are spheres, the total projected surface area concentration in a suspension is

$$A_T = \int_{D_{\min}}^{D_{\max}} n(D) \frac{\pi D^2}{4} dD. \tag{3}$$

In Eq. (3), A_T ($\mathrm{m}^2\ \mathrm{m}^{-3}$, i.e., m^{-1}) is the total projected area concentration, and $D_{\max}$ and $D_{\min}$ (m) are the upper and lower diameters of the particle size range as determined by the instrument used to measure area. Insertion of Eq. (2) into Eq. (3) yields

$$A_T = \frac{n_c \pi D_c^2}{4} \int_{D_{\min}}^{D_{\max}} \left(\frac{D}{D_c} \right)^{2-b} dD. \tag{4}$$

Table 1
Notation.

Symbol	Definition, units
A	LISST total area concentration, m^{-1}
A_i	LISST area concentration in size class i, m^{-1}
A_T	Total projected area concentration, m^{-1}
b	Exponent in power-law size distribution, dimensionless
D	Particle diameter, m
D_c	Diameter of component particles in aggregates, m
D_{cm}	Diameter of component mineral particles in aggregates, m
D_{co}	Diameter of component organic particles in aggregates, m
D_i	LISST diameter of size class i, μm
$D_{\max}$	Maximum particle diameter in suspension, m
$D_{\min}$	Minimum particle diameter in suspension
$D3$	3-D fractal dimension
$D3_m$	3-D fractal dimension of mineral particles
$D3_o$	3-D fractal dimension of organic particles
F	F statistic, dimensionless
LISST	Laser In Situ Size and Scattering Transmissometer
M	Particle mass, kg
M_c	Mass of component particles in aggregates, kg
MSM	Mineral suspended mass concentration, g m^{-3}
$n(D)$	Particle number concentration, m^{-4}
n_c	Number concentration of component particles, m^{-4}
OSM	Organic suspended mass concentration, g m^{-3}
p	Number of predictor variables in the full model (= 2), dimensionless
q	Number of predictor variables in the reduced model (= 1), dimensionless
R_f	Multiple correlation coefficient from the full model, dimensionless
R_r	Correlation coefficient from the reduced model, dimensionless
TSM	Total suspended mass concentration, kg m^{-3}
V_i	LISST volume concentration in size class i, ppm
β_c	Constant regression coefficient, m^{-1}
β_{cL}	Large particle area uncorrelated with LISST area, m^{-1}
β_L	Coefficient of proportionality between LISST area and total area, dimensionless
β_m	Mineral area-to-mass ratio estimated by regression, $m^2\ g^{-1}$
β_o	Organic area-to-mass ratio estimated by regression, $m^2\ g^{-1}$
β_{rc}	Constant regression coefficient in the reduced model, m^{-1}
β_{rm}	Area-to-mass ratio in the reduced model, $m^2\ g^{-1}$
ε	Random error term in regression, m^{-1}
ε_L	Random error term in relationship between LISST and total area, m^{-1}
ε_r	Random error term in the reduced model, m^{-1}
$\rho(D)$	Particle density, kg m^{-3}
ρ_c	Component particle density, kg m^{-3}
ρ_{cm}	Component mineral particle density, kg m^{-3}
ρ_{om}	Component organic particle density, kg m^{-3}

Upon integration and under the assumption that $D_{\min} = D_c$, Eq. (4) becomes

$$A_T = \frac{n_c \pi D_c^3}{4\,(b-3)} \left[1 - \left(\frac{D_{\max}}{D_c} \right)^{3-b} \right]. \tag{5}$$

Observed values of b typically fall between 3.5 and 5 (e.g., Stemmann and Boss, 2012), and for the purposes of illustration, a constant value of 4 is used here. With $b = 4$, Eq. (5) becomes

$$A_T = \frac{n_c \pi D_c^3}{4} \left[1 - \left(\frac{D_{\max}}{D_c} \right)^{-1} \right]. \tag{6}$$

Because $D_{\max}$ is typically much greater than D_c, Eq. (6) essentially states that the projected area concentration depends on the concentration and size of the smallest particles in suspension.

The total suspended mass is derived similarly to the projected area concentration:

$$TSM = \int_{D_{\min}}^{D_{\max}} \rho(D) n(D) \frac{\pi D^3}{6} dD. \tag{7}$$

In Eq. (7), TSM (kg m^{-3}) is total suspended mass concentration, and $\rho(D)$ (kg m^{-3}) is the apparent density of particles of diameter D. Apparent density equals the solid-mass-to-wet-volume ratio of a particle, and with the fractal model it is defined by the equation (cf. Maggi, 2013):

$$\rho(D) = \rho_c \left(\frac{D}{D_c} \right)^{D3-3}. \tag{8}$$

In Eq. (8) ρ_c (kg m^{-3}) is the apparent density of the component grains. Insertion of Eqs. (2) and (8) into Eq. (7) yields

$$TSM = \frac{n_c \rho_c \pi D_c^3}{6} \int_{D_{\min}}^{D_{\max}} \left(\frac{D}{D_c} \right)^{D3-b} dD. \tag{9}$$

Proceeding under the assumption that $D_{\min} = D_c$, the integral becomes

$$TSM = \frac{n_c \rho_c \pi D_c^4}{6(b - D3 - 1)} \left[1 - \left(\frac{D_{\max}}{D_c} \right)^{D3+1-b} \right]. \tag{10}$$

If $b = 4$, then

$$TSM = \frac{n_c \rho_c \pi D_c^4}{6(3 - D3)} \left[1 - \left(\frac{D_{\max}}{D_c} \right)^{D3-3} \right]. \tag{11}$$

By applying the reasonable assumption that $D_{\max} \gg D_c$, Eqs. (6) and (11) can be combined to form an illustrative, albeit simplified, expression for the area-to-mass ratio in a suspension:

$$A_T : TSM = \frac{3(3 - D3)}{2\rho_c D_c}. \tag{12}$$

Eq. (12) suggests that $A_T : TSM$ responds most strongly to three particle parameters, which are the component particle density, the component particle diameter, and the fractal dimension, or packing geometry, of aggregates. Smaller values of component particle density or diameter produce larger projected-area-to-mass ratios. Smaller values of the fractal dimension, which are associated with more loosely packed aggregates, also produce larger projected-area-to-mass ratios.

The simplified expression for the projected-area-to-mass ratio (Eq. (12)) can be used to characterize sources of difference in the ratios for organic matter versus inorganic (mineral) matter. Using the subscripts o and m for organic and inorganic mineral matter, respectively, the ratio of organic projected-area-to-mass ratio to mineral projected-area-to-mass ratio is

$$\frac{(A_T : TSM)_o}{(A_T : TSM)_m} = \frac{(3 - D3_o)\, \rho_{cm} D_{cm}}{(3 - D3_m)\, \rho_{co} D_{co}}. \tag{13}$$

Eq. (13) shows that the projected-area-to-mass ratios of organic and mineral matter will differ simply because the density of mineral matter is roughly 2 times larger than that of organic matter (cf., Babin et al., 2003). As a result, if one assumes that the component diameters or fractal dimensions of organic and inorganic matter are the same, the projected-area-to-mass ratio for organic matter will be approximately twice as large as that for mineral matter. Babin et al. (2003) used this argument implicitly to explain the factor-of-two difference between mass-specific scattering coefficients in oceanic waters, where particles are predominantly organic, versus in coastal waters, where suspended particles are more inorganic.

Differences in the component particle diameters of organic and mineral matter can cause the projected-area-to-mass ratios to differ. If organic component particles are smaller than mineral component particles, then the projected-area-to-mass ratio of organic matter can be more than twice as large as the projected-area-to-mass ratio of mineral matter. Similarly, if organic component particles are larger than mineral component particles, then the projected-area-to-mass ratio of organic matter can be less than twice as large as the projected-area-to-mass ratio of mineral matter. Differences in fractal dimension between organic and inorganic particles also can affect area-to-mass ratios. Stickier particles clump to produce aggregates with lower fractal dimensions than less sticky particles (e.g., Lin et al., 1989). Therefore, organic-rich particles, if they are stickier than mineral particles, may produce aggregates with lower fractal dimensions than mineral-rich aggregates, potentially giving them larger area-to-mass ratios (Braithwaite et al., 2010; Logan and Wilkinson, 1990). The reverse would result if organic-rich aggregates were packed more tightly than mineral aggregates.

The preceding analysis produces some useful, testable predictions. If there are no systematic correlations between component particle composition and component particle diameter or fractal dimension, then the projected-area-to-mass ratio for organic matter is approximately twice that of inorganic matter. If correlations exist, then the area-to-mass ratio for organic matter will be statistically different from twice the value of the area-to-mass ratio for inorganic matter. Alternatively, violation of the simplifying assumptions on which Eq. (12) is based could cause the area-to-mass ratio for organic matter to be statistically different from twice the value of the area-to-mass ratio for inorganic matter. In this study, observations of suspended particle mass and area concentrations are combined with observations of organic and inorganic content to test the null hypothesis that the area-to-mass ratio of organic matter is twice as large as the area-to-mass ratio of inorganic matter.

Methods

The data comprise optical measurements of particle area paired with gravimetric measurements of particle mass. Two different Sequoia Scientific LISST100X sensors were used to measure the particle area. A LISST100X Type C was used for all measurements except those in the Menai Strait, for which a Type B sensor was used. Bucket samples of water were collected and subsequently filtered to estimate the mass in suspension. The data were collected in moderately turbid waters at sites along the west and south coasts of Great Britain during 2008 and 2009.

The majority of the data derive from three sites: the Menai Strait, which separates the island of Anglesey from the mainland in northwest Wales, the Tamar estuary and adjacent Plymouth Sound in southwest England, and the Irish Sea north of Anglesey. Other sites include Conwy Bay on the north coast of Wales, and Solway Firth, Burrows Head, and Inchmarnock Water, all located on the southwest coast of Scotland (Fig. 1).

The Menai Strait is a narrow, rocky channel with rectilinear tidal flow and strong temporal gradients of turbulence associated with tidal and spring-neap cycles (Bowers et al., 2009). The water column is well mixed. Measurements were conducted during a spring tide and during a neap tide. The neap tide samples were gathered after a large rainfall event that resulted in significant discharge of sediment into coastal waters. Because of the different tidal stages and the runoff event, the two sets of samples from the Menai Strait were treated as different "sites" in the statistical analysis.

The Tamar Estuary is situated on the southwest coast of England forming a boundary between the counties of Devon and Cornwall. It discharges into Plymouth Sound. Measurements were collected on a longitudinal transect of the lower estuary, extending from 9 km up-estuary to the bar in Plymouth Sound. The estuary is mesotidal, with a mean tidal range of 3.5 m. Annual mean discharge is 2.7 $m^3\ s^{-1}$ (Braithwaite et al., 2010). Given the relatively large tidal range and small discharge, waters were either vertically well mixed or weakly stratified during sampling. Water depths varied from 10 to 20 m along the transect.

The Irish Sea north of Anglesey is characterized by strong tidal streams, with currents reaching 2 m s^{-1}. Observations were made at a site with a water depth of 30 m, and the water was well mixed. The Irish Sea in this area is productive, and some of the measurements were characterized by high chlorophyll concentrations associated with a bloom of diatoms. As with the Menai Strait data, the high-chlorophyll data were treated as a different site in the statistical analysis.

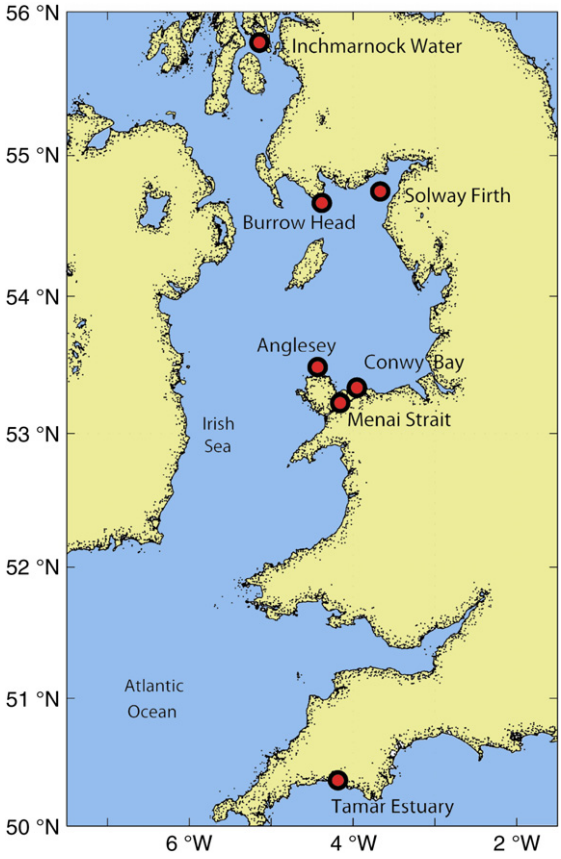

Fig. 1. Locations of sample sites.

The LISST measured scattering intensity on a set of ring detectors. The intensity and distribution of scattered light were converted to volume concentration in 32 size classes with an instrument-specific calibration coefficient and with the manufacturer's spherical matrix. The volume concentrations are given in parts per million. The resolvable size range for the Type C is 2.50–500 μm, and it is 1.25–250 μm for the Type B.

The LISST was lowered through the water column to a depth of ten meters for the Irish Sea coastal stations, and it was lowered to the bottom in the Tamar Estuary and in the Menai Strait. Depth-averaged volume concentrations for each cast were generated by summing the volume in each size class and dividing by the number of size distributions measured during the cast. Assuming spherical geometry, depth-averaged volume concentration in size class i (V_i, ppm) was converted to depth-averaged area concentration in size class i (A_i, m^{-1}) according to the equation

$$A_i = \frac{3V_i}{2D_i}, \tag{14}$$

where D_i is the diameter of size class i (μm). Depth-averaged total suspended area concentration (A) was calculated by summing areas in the 32 size classes.

Surface water was collected in a bucket at each station to estimate total suspended mass (TSM). Because the water column at the various sites was well-mixed to the depths of the profiles, these surface samples were assumed to be representative of the entire profile. Gravimetric determinations of TSM concentration were made following standard protocols (Kratzer et al., 2000). Known volumes

of water were vacuum-pumped through pre-weighed Whatman GF/F filters (0.7 μm pore size). The filters were prepared by washing in distilled water and drying in a muffle furnace for 3 h at 500 °C prior to weighing. After the suspensate was drawn through the filters, the filters, including the filter rims, were rinsed with 250 ml of distilled water. *TSM* was determined by drying and weighing the filters. Then the filters were baked for 3 h at 500 °C to remove organic material and re-weighed to give the concentration of Mineral Suspended Mass (*MSM*). Organic Suspended Mass (*OSM*) was calculated by subtracting *MSM* from *TSM*.

It is important to note that the lower and upper bounds of the size distribution of area as measured by the LISST differ from the lower and upper bounds of the size distribution of mass measured gravimetrically. The LISST lower limit of resolution is 1.25 μm for the Type B and 2.50 μm for the Type C, but filtration nominally traps particles as small as 0.7 μm and in practice traps even smaller particles once filters are loaded with sediment (Sheldon, 1972). The upper limits of resolution of the LISST instruments are 250 and 500 μm respectively for the Types B and C, but filtration can capture larger particles. The different limits of resolution mean that if there are particles smaller or larger than the LISST can detect, then underestimation of the absolute values of area-to-mass ratios will result. If, however, the particle area concentrations measured by the LISST are proportional to the area concentrations of particles smaller or larger than the LISST limits of resolution, then the relative magnitudes of the area-to-mass ratios of organic and inorganic matter should be accurate. The analysis proceeds under this assumption, which is evaluated further in the discussion.

To investigate the effect of composition on the particle area-to-mass ratio, multiple linear regression was used to quantify the dependence of total suspended area on organic suspended mass and mineral suspended mass, according to the equation

$$A = \beta_c + \beta_o OSM + \beta_m MSM + \varepsilon. \tag{15}$$

In Eq. (15) the β terms are regression coefficients, where the subscripts c, o, and m refer to the coefficients for the constant term, the organic mass term, and the mineral mass term, respectively. The coefficient β_c gives the value of area concentration when OSM and MSM are zero. It has units of m^{-1} (i.e., $m^2\ m^{-3}$), and ideally it is not statistically different from zero. The units of β_o and β_m are $m^2\ g^{-1}$ because they quantify the change in area that arises from unit changes in OSM and MSM, respectively, when the other mass variable is held constant (Chatterjee and Hadi, 2012). The magnitude of the change in area from a unit change in OSM does not depend on the value at which MSM is fixed, and vice versa. Therefore it is valid to interpret the coefficients as estimates of the area-to-mass ratios of OSM and MSM. The error term ε represents random variations in A.

Babin et al.'s (2003) hypothesis that $\beta_o = 2\beta_m$ was employed as a null hypothesis and used to construct a reduced model with which to evaluate that null hypothesis statistically. The reduced model takes the form

$$\begin{aligned} A &= \beta_{rc} + \beta_{rm}(2OSM + MSM) + \varepsilon_r, \quad \text{or} \\ A &= \beta_{rc} + \beta_{rm} X + \varepsilon_r, \end{aligned} \tag{16}$$

where the subscript r refers to coefficients associated with the reduced model. The null hypothesis was evaluated via the F statistic, defined as (Chatterjee and Hadi, 2012)

$$F = \frac{\left(R_f^2 - R_r^2\right) / (p - q)}{\left(1 - R_f^2\right) / (n - p - 1)}. \tag{17}$$

In Eq. (17) R_f is the multiple correlation coefficient from the full model, and R_r is the correlation coefficient from the reduced model. The variable p (= 2) is the number of predictor variables in the full model, and q (= 1) is the number of predictor variables in the reduced model. The variable n is the number of observations. The value of F was compared to the tabulated value of $F_{(p-1,n-p-1,0.05)}$. If the computed F was larger than the tabulated value, then the null hypothesis that $\beta_o = 2\beta_m$ was rejected.

The robustness of the results of the regression analysis was evaluated in three ways. First, the effect of influential points was assessed by identifying and removing these points from the analysis. These points were identified with a potential-residual plot (Hadi, 1992). Second, the influence of individual

Table 2
Regression coefficients with 95% confidence intervals and associated R^2 values for full and reduced models. Results report values with all data and with identified influence points omitted.

Model	n	β_c ($m^2\ m^{-3}$)	β_o ($m^2\ g^{-1}$)	β_m ($m^2\ g^{-1}$)	R^2
Full model	92	-0.145 ± 0.137	0.160 ± 0.097	0.119 ± 0.025	0.685
Reduced model	92	-0.106 ± 0.133		0.135 ± 0.020	0.672
Full model without influence points	88	-0.167 ± 0.107	0.191 ± 0.096	0.117 ± 0.022	0.791
Reduced model without influence points	88	-0.175 ± 111		0.111 ± 0.012	0.790

Table 3
Sample size, R^2 values for the full and reduced models, ratio of organic to mineral area-to-mass ratios, associated F statistics, and critical F values for regression models with a site deleted. Because F stat $<$ F crit for each model, the hypotheses that $\beta_o = 2\beta_m$ cannot be rejected with the full data set or when any individual site is omitted from the analysis.

Omitted site	n	R_f^2	R_r^2	β_o/β_m	F stat	F crit
None	92	0.685	0.672	1.34	3.61	3.94
Menai Strait, neap	79	0.630	0.629	2.34	0.19	3.96
Menai Strait, spring	85	0.596	0.585	1.20	2.20	3.95
Tamar	62	0.793	0.791	1.35	0.73	4.00
Conwy bay	90	0.688	0.683	1.32	1.48	3.95
Solway firth	80	0.729	0.724	1.35	1.32	3.96
Burrow head	84	0.663	0.654	1.14	2.15	3.95
Inchmarnock water	91	0.686	0.682	1.34	1.38	3.94
Anglesey, bloom	87	0.685	0.680	1.28	1.49	3.95
Anglesey, time series	78	0.667	0.658	1.16	1.88	3.96

sites on the results was assessed by systematically removing a site from the data and then conducting the statistical analysis on the pruned data set. Finally, due to concern with the accuracy of LISST estimates of small particle concentration (e.g., Neukermans et al., 2012), the smallest 5 size classes of the LISST Type B data were eliminated from the analysis.

Results and discussion

The full model (Eq. (15)) provided a statistically significant fit to the data ($p = 0$, Fig. 2). The values of β_o and β_m were 0.160 ± 0.097 and 0.119 ± 0.025 $m^2\ g^{-1}$ respectively (Table 2). The 95% confidence intervals on the slopes are included. The model explained more than two thirds of the observed variability in the total suspended area ($R_f^2 = 0.685$, Table 2). The fit of the reduced model was not statistically worse than the full model (Tables 2 and 3), and the value of β_{rm} was 0.135 ± 0.020 $m^2\ g^{-1}$ (Table 2). The null hypothesis that $\beta_o = 2\beta_m$ was not rejected. A reasonable inference from this result is that particle composition was not correlated with component particle size or aggregate packing geometry (Eq. (13)).

The potential-residual plot revealed 4 points of influence (Fig. 3). Point 48 had high leverage, and points 15, 21, and 59 were outliers (Hadi, 1992). Points 21 and 48 were located at the landward end of the Tamar Estuary transect. Point 15 was collected in the Menai Strait during the spring-tide sampling effort, and point 59 was from Solway Firth. Omission of these points did not alter the fundamental result that the null hypothesis could not be rejected. The values of β_o and β_m were 0.191 ± 0.096 and 0.117 ± 0.022 $m^2\ g^{-1}$ respectively (Table 2). The removal of the outliers naturally produced a better fit of the model to the data ($R_f^2 = 0.791$, Table 2). The value of β_{rm} was 0.111 ± 0.012 $m^2\ g^{-1}$, and $R_r^2 = 0.790$ (Table 2). Omission of individual sites from the analysis did not change the fundamental result that the null hypothesis could not be rejected (Table 3). Finally, omission of the first 5 size bins from the Type B data also did not allow rejection of the null hypothesis (not shown).

The area-to-mass ratios for organic and mineral suspended mass estimated from this study were 0.16 and 0.12 $m^2\ g^{-1}$. Under the assumption that the scattering and attenuation efficiencies equal 2, a doubling of the area-to-mass ratios for organic and mineral suspended solids should give the mass-specific attenuation and scattering coefficients for organic and mineral matter. The resulting

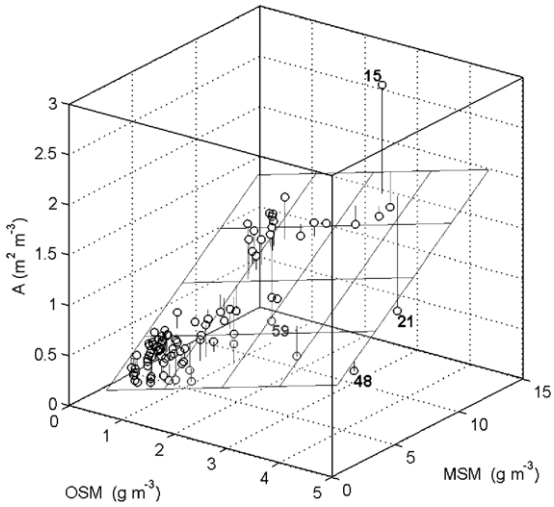

Fig. 2. Data and best-fit multiple linear regression of total suspended area on organic suspended mass and mineral suspended mass. Numbered points are influential, either because they have high leverage (48) or because they are outliers (15, 21, 59).

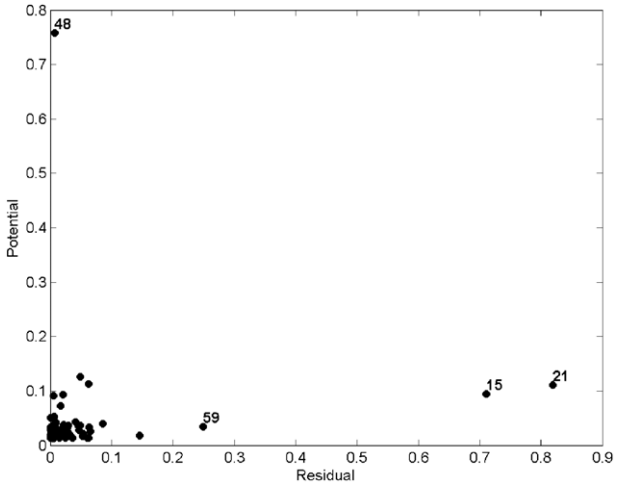

Fig. 3. Potential-residual plot. Points with large potentials have large leverage, and points with large residuals are potential outliers. Numbered points indicate the points omitted in the analysis of the influence of individual points on the overall results of the regression analysis. Point 15 is one of the Menai Strait, spring-tide observations, Point 21 and 48 are from the landward end of the Tamar estuary transect, and point 59 is one of the Solway Firth observations.

values of 0.32 and 0.24 are at the lower range of mass-specific scattering and attenuation coefficients measured in organic-rich oceanic waters and mineral-rich coastal waters (e.g., Hill et al., 2011; Babin et al., 2003; Wozniak et al., 2010). These relatively low area-to-mass ratios suggest that measured areas were underestimates and/or that measured masses were overestimates.

LISST instruments have been shown to provide reasonably accurate size distributions for an array of different particle types (e.g., Karp-Boss et al., 2007; Reynolds et al., 2010). LISST instruments also possess known sources of error, which are summarized by Andrews et al. (2010). First, the inversion matrices required to convert the intensity of scattered light on the instrument ring detectors into particle concentrations make assumptions about particle properties, most importantly particle shape

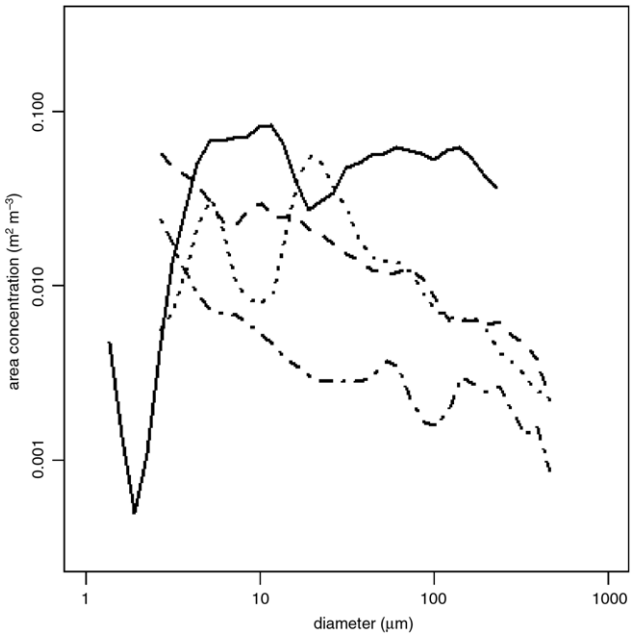

Fig. 4. Representative averaged LISST area concentrations versus diameter from 4 sites: solid line, Menai Strait, neap observations; dashed line, Tamar estuary; dashed–dotted line, Burrow Head; *dotted line*, Anglesey bloom observations. The size distributions differ but have no apparent correlation with the composition of the suspension. The Menai Strait and Burrow Head had the largest mineral fractions in the study, with median *TSM/MSM* approximately equal to 0.85. The Anglesey bloom observations had the smallest mineral fractions, with a median value around 0.65. The Tamar median mineral fraction was intermediate to these values.

and composition (Karp-Boss et al., 2007; Andrews et al., 2010; Agrawal et al., 2008; Davies et al., 2012; Graham et al., 2012). Second, stray light can affect estimates of particle size distribution (Reynolds et al., 2010; Andrews et al., 2011). Finally, LISST instruments have finite size ranges that do not necessarily cover the full in situ size distribution (Andrews et al., 2010; Davies et al., 2012).

Small, non-spherical particles scatter light at wider angles than spherical particles, making it appear as if more small particles exist (Agrawal et al., 2008). In acute cases, this effect can cause marked, rising tails in particle size distributions. An empirical random-shape inversion matrix was developed to deal with suspensions in which there are abundant, platy, small particles (Agrawal et al., 2008). The general lack of large-magnitude, rising fine tails in this study (Fig. 4) indicated that irregular shape of small particles was not a significant problem, justifying the application of the spherical inversion matrix. As well, the elimination of the smallest 5 size classes from the LISST Type B data from the Menai Strait, which would have been affected most by random-shape effects, did not result in rejection of the null hypothesis. Natural large aggregates with complex shapes likely produce complex scattering patterns that LISST interprets as multiple particle size classes (Graham et al., 2012). Complex scattering patterns may cause LISST to overestimate particle concentrations, especially at the fine end of the size distribution (Graham et al., 2012). Large, orders-of-magnitude overestimation of volume by the LISST described by Graham et al. (2012), however, were unlikely in this study because area-to-mass ratios were of the appropriate order of magnitude.

Particle composition determines the refractive index, and the refractive index affects the magnitude of scattering, particularly for particles $<$ 20 μm (Andrews et al., 2010). As a result, mismatch between actual and assumed refractive indices causes inaccurate estimates of small particle concentrations. Applying refractive indexes typical of mineral matter produces the most accurate estimates of particle concentration, even in suspensions of phytoplankton (Andrews et al., 2010). Andrews et al. (2010) argue that particles with low bulk indexes of refraction may scatter more

intensely than assumed because of internal structure, and this effect may explain why LISSTs, which assume a relatively large refractive index, provide generally accurate results in a wide range of suspension compositions.

Ambient light can reduce the accuracy of LISST concentrations. Ambient light impinges primarily on the outer ring detectors, so it can cause a rising fine tail in particle size distributions (Reynolds et al., 2010; Andrews et al., 2011). The problem is most acute for the outer 5 rings of the LISST Type B (Andrews et al., 2011). This problem has led some investigators to remove the smallest size classes from LISST particle size distributions (Neukermans et al., 2012; Reynolds et al., 2010). Again, the elimination of the smallest 5 size classes from the LISST Type B data from the Menai Strait did not result in rejection of the null hypothesis, suggesting that ambient light contamination was not a problem. This result may have been due to the relatively large turbidity of water in the Menai Strait.

The limited range of resolution of the LISST can cause estimates of area to be in error. The LISST B does not detect particles smaller than 1.25 μm or larger than 250 μm, and the LISST C does not detect particles smaller than 2.5 μm or larger than 500 μm. Particles smaller than the lower limit of resolution of LISST exist, but concentrations are not well known. Recent work suggests that particles below the resolution limits of LISST sensors are not abundant (Andrews et al., 2010; Graham et al., 2012; Peng and Effler, 2007). Scavenging of small particles by aggregates may explain low small particle abundances (Graham et al., 2012; Eisma et al., 1990; Flory et al., 2004). Aggregates larger than 250 or 500 μm are common in suspension and can contribute significantly to the total area (Mikkelsen et al., 2006; Hatcher et al., 2001).

The presence of small, out-of-range particles can affect the entire size distribution (Andrews et al., 2010). Their presence increases the estimated abundance of particles in LISST's smallest size classes, and the increase in volume can be of the same magnitude as the volume of the out-of-range particles (Reynolds et al., 2010; Andrews et al., 2010). Small, out-of-range particles can also create area in the largest LISST size classes and decrease area in mid-range size classes (Andrews et al., 2010). These effects are not large if the concentrations of natural, out-of-range particles are small (Andrews et al., 2010; Graham et al., 2012; Peng and Effler, 2007).

The presence of large, out-of-range particles primarily affects the largest size classes (Andrews et al., 2010; Davies et al., 2012). Secondary and tertiary scattering peaks of large, out-of-range particles are intense enough to affect volume estimates (Davies et al., 2012). Large, out-of-range particles also cause scattering at large angles, an effect that generates spurious small particles (Davies et al., 2012). For typical size distributions, however, these effects should not be large (Andrews et al., 2010; Davies et al., 2012).

In summary, there is no strong evidence that the areas measured by LISST were in error because of irregular shape, variable composition, ambient light contamination or out-of-range particles. Although the LISST area concentrations over the measured size range likely were accurate, the total areas measured by LISST likely were underestimates of total area because of the presence of out-of-range particles.

The consequences of the inability of the LISST to resolve the entire particle size range can be explored by considering a linear relationship between the suspended area concentration measured by the LISST (A, $\mathrm{m^2\ m^{-3}}$) and the total suspended area concentration, termed A_T ($\mathrm{m^2\ m^{-3}}$). Suppose some portion of the total area was linearly related to the LISST area, and another portion of the total area was uncorrelated. Under these assumptions

$$A = \beta_L A_T - \beta_{cL} + \varepsilon_L \tag{18}$$

where β_L ($\mathrm{m^2\ m^{-2}}$) denotes the change in the LISST area caused by a unit change in total area, and β_{cL} ($\mathrm{m^{-1}}$) is the portion of the total area that is not correlated with the area measured by LISST. The term ε_L is the random error. The substitution of Eq. (18) into Eq. (15) yields

$$\beta_L A_T - \beta_{cL} + \varepsilon_L = \beta_c + \beta_o OSM + \beta_m MSM + \varepsilon, \tag{19}$$

which can be rearranged to provide an expression for the total area:

$$A_T = \left(\frac{\beta_c + \beta_{cL}}{\beta_L}\right) + \left(\frac{\beta_o}{\beta_L}\right) OSM + \left(\frac{\beta_m}{\beta_L}\right) MSM + \left(\frac{\varepsilon + \varepsilon_L}{\beta_L}\right). \tag{20}$$

The first term on the right hand side of Eq. (20) expresses the total suspended particle area in the absence of suspended organic and mineral mass. Clearly, this term should equal zero, so

$$\beta_{cL} = -\beta_c. \tag{21}$$

The value of β_c from the regression of A on OSM and MSM (Eq. (15)) was -0.145 ± 0.137 m^2 m^{-3} (Table 2), which was significantly different from zero ($p = 0.0382$). This result suggests that, on average, a fraction of the total suspended area was uncorrelated with the area resolved by the LISST. The median value of (β_c/A), which is an estimate of this fraction, equals 0.26. Under the assumption that this fraction is not correlated differently with organic and mineral mass, Eq. (20) demonstrates that the magnitudes of the regression coefficients would differ from those obtained with Eq. (15), but the ratio of the magnitudes would not. As a result, the comparison of area-to-mass ratios in this study should be valid despite the inability of the LISST to measure the entire size spectrum. Eq. (20) also demonstrates that if half of the total area was in the LISST size range, then total area-to-mass ratios would be twice as large as the coefficients estimated with the LISST. This magnitude of change would produce mass-specific attenuation coefficients typically observed in coastal waters (e.g., Babin et al., 2003; Wozniak et al., 2010).

Error in the estimation of suspended mass concentration can also explain the relatively low area-to-mass ratios. Salt retention is the most likely source of over-estimation of suspended mass via filtration (Stavn et al., 2009). The filters in this study were all rinsed with 250 ml of distilled water (Wozniak et al., 2010), which is close to the value of 300 ml documented by Stavn et al. (2009) to leave 0.5 to 1 mg of salt on filters depending on salinity of the original sample. Given the total suspended masses in this study, which are similar to the values considered by Stavn et al. (2009), salt retention would have produced absolute errors in masses of 20% or less. This error helps to explain why area-to-mass ratios are lower than expected. More importantly, Stavn et al. (2009) also showed that a unit change in suspended particulate mass uncorrected for the retention of salt produces a unit change in corrected suspended particulate mass. This finding indicates that salt retention would not have changed the slopes of the relationships between area and suspended mass, so the comparison of area-to-mass ratios in this study remains valid despite salt retention.

The foregoing analysis provides no clear indication of error in the failure to reject the null hypothesis. This result can be used to infer that particle composition is not correlated with particle size or packing geometry. Other studies, however, suggest that such correlations do exist. By fitting a model of particle settling velocity to data sets divided broadly into biological, bio-mineral and mineral aggregates, Maggi (2013) found differences in estimated component-particle density, component-particle size, and aggregate packing geometry among the three groups. Mineral aggregates had larger component particles with larger densities than biological aggregates. Interestingly, estimated fractal dimensions for mineral aggregates across the size spectrum were relatively constant at a value 2.3, whereas estimated fractal dimensions for biological aggregates were 2.9 for component particles, but decreased to values similar to mineral aggregates for diameters of several hundred micrometers. These results reveal potentially offsetting effects of component particle size and aggregate packing geometry (Eq. (13)). Larger component particles in mineral aggregates would push the ratio of organic and mineral area-to-mass ratios higher than 2. Larger fractal dimensions of organic aggregates, in contrast, would reduce the area-to-mass ratios. These results offer an alternative explanation for the failure to reject the null hypothesis. Aggregate packing geometry and component particle size may be correlated with particle composition, but the correlations produce effects of opposite sign. The result is that the ratio of organic area-to-mass ratio to mineral area-to-mass ratio is not significantly different from 2.

Wozniak et al. (2010) used an extensive time series of optical and particle properties at a coastal site in California to assess the effect of particle composition on mass-specific scattering coefficients. They observed that mineral-rich and organic-rich suspensions both had variable mass-specific scattering coefficients but also that the magnitudes were not dramatically different. They argued that the finer particle size distributions typical of mineral-rich waters offset the effect of larger particle density. The effect of different organic and mineral size distributions was neglected in the simplified theory presented here, partly due to apparent lack of correlation between composition and the size distributions measured in this study (Fig. 4). Again, observed correlations between composition and size may be too weak to produce organic area-to-mass ratios that are statistically different from

two times larger than mineral area-to-mass ratios. Clearly, measurements of the full particle size distribution, paired with explicit investigations of correlation among particle packing and component particle composition and size are required to quantify and constrain the sources of variability in mass-specific optical coefficients more fully.

Conclusion

Data from the south and west coasts of Great Britain did not allow the rejection of the null hypothesis that organic matter possesses projected-area-to-mass ratios that are two times larger than the projected-area-to-mass ratios of mineral matter (Babin et al., 2003). The order-of-magnitude variability in published mass-specific attenuation coefficients cannot be attributed to composition alone, and the previous work indicates that it also cannot be attributed to variable particle size in suspension (Hill et al., 2011; Neukermans et al., 2012; Boss et al., 2009). A large fraction of observed variability must be due, therefore, either to variations in the diameter of component particles that make up aggregates or the packing geometry of aggregates. The failure to reject the null hypothesis may indicate that variations in component particle size and aggregate packing geometry are uncorrelated with particle composition. Alternatively, it may indicate that correlations between component particle composition, component particle size, and aggregate packing geometry produce unresolved, offsetting effects that leave organic area-to-mass ratios near to values that are twice the magnitude of mineral area-to-mass ratios.

Acknowledgments

This work was initiated by a Kirby Laing Fellowship awarded to PSH by Bangor University. Further funding for the research was provided to PSH by the United States Office of Naval and to DGB and KMB by NERC and dstl in the United Kingdom. PSH extends warm thanks to Samprit Chatterjee for providing statistical advice and tea on his porch in Brooksville, Maine.

References

Agrawal, Y.C., Whitmire, A., Mikkelsen, O.A., Pottsmith, H.C., 2008. Light scattering by random shaped particles and consequences on measuring suspended sediments by laser diffraction. J. Geophys. Res. Oceans 113 (C4), C04023. http://dx.doi.org/10.1029/02007JC004403.

Andrews, S.W., Nover, D.M., Reardon, K.E., Reuter, J.E., Schladow, S.G., 2011. The influence of ambient light intensity on in situ laser diffractometers. Water Resour. Res. 47, W06509. http://dx.doi.org/10.1029/2010WR009841.

Andrews, S., Nover, D., Schladow, S.G., 2010. Using laser diffraction data to obtain accurate particle size distributions: the role of particle composition. Limnol. Oceanogr. Methods 8, 507–526.

Babin, M., Morel, A., Fournier-Sicre, V., Fell, F., Stramski, D., 2003. Light scattering properties of marine particles in coastal and open ocean waters as related to the particle mass concentration. Limnol. Oceanogr. 48, 843–859.

Baker, E.T., Lavelle, J.W., 1984. The effect of particle size on the light attenuation coefficient of natural suspensions. J. Geophys. Res.-Oceans 89, 8197–8203.

Beardsley, G.F., Pak, H., Carder, K., Lundgren, B., 1970. Light scattering and suspended particles in the Eastern Equatorial Pacific Ocean. J. Geophys. Res. 75, 2837–2845.

Boss, E., Slade, W., Hill, P., 2009. Effect of particulate aggregation in aquatic environments on the beam attenuation and its utility as a proxy for particulate mass. Opt. Express 17, 9408–9420.

Bowers, D.G., Braithwaite, K.M., Nimmo-Smith, W.A.M., Graham, G.W., 2009. Light scattering by particles suspended in the sea: the role of particle size and density. Cont. Shelf Res. 29, 1748–1755.

Braithwaite, K.M., Bowers, D.G., Smith, W.A.M.N., Graham, Agrawal, G W, Mikkelsen, Y C, O.A., 2010. Observations of particle density and scattering in the Tamar Estuary. Mar. Geol. 277, 1–10.

Burd, A.B., Jackson, G.A., 2009. Particle aggregation. Annu. Rev. Mar. Sci. 1, 65–90.

Chatterjee, S., Hadi, A.S., 2012. Regression Analysis by Example, fifth ed. John Wiley & Sons, Hoboken, New Jersey, p. 393.

Davies, E.J., Nimmo-Smith, W.A.M., Agrawal, Y.C., Souza, A.J., 2012. LISST-100 response to large particles. Mar. Geol. 307–310, 117–122.

Downing, J., 2006. Twenty-five years with OBS sensors: the good, the bad, and the ugly. Cont. Shelf Res. 26, 2299–2318.

Eisma, D., Schuhmacher, T., Boekel, H., Vanheerwaarden, J., Franken, H., Laan, M., Vaars, A., Eijgenraam, F., Kalf, J., 1990. A camera and image analysis system for in situ observations of flocs in natural waters. Neth. J. Sea Res. 27, 43–56.

Flory, E.N., Hill, P.S., Milligan, T.G., Grant, J., 2004. The relationship between floc area and backscatter during a spring phytoplankton bloom. Deep-Sea Res. I 51, 213–223.

Fugate, D.C., Friedrichs, C.T., 2002. Determining concentration and fall velocity of estuarine particle populations using ADV, OBS and LISST. Cont. Shelf Res. 22, 1867–1886.

Graham, G.W., Davies, E.J., Nimmo-Smith, W.A.M., Bowers, D.G., Braithwaite, K.M., 2012. Interpreting LISST-100X measurements of particles with complex shape using digital in-line holography. J. Geophys. Res. 117, C05034. http://dx.doi.org/10.1029/2011JC007613.
Hadi, A.S., 1992. A new measure of overall potential influence in linear regression. Comput. Statist. Data Anal. 14, 1–27.
Hatcher, A., Hill, P., Grant, J., 2001. Optical backscatter of marine flocs. J. Sea Res. 46, 1–12.
Hill, P.S., Boss, E., Newgard, J.P., Law, B.A., Milligan, T.G., 2011. Observations of the sensitivity of beam attenuation to particle size in a coastal bottom boundary layer. J. Geophys. Res.-Oceans 116.
Karp-Boss, L., Azevedo, L., Boss, E., 2007. LISST-100 measurements of phytoplankton size distribution: evaluation of the effects of cell shape. Limnol. Oceanogr.-Methods 5, 396–406.
Khelifa, A., Hill, P.S., 2006. Models for effective density and settling velocity of flocs. J. Hydraul. Res. 44, 390–401.
Kitchen, J.C., Zaneveld, J.R.V., Pak, H., 1982. Effect of particle-size distribution and chlorophyll content on beam attenuation spectra. Appl. Opt. 21, 3913–3918.
Kratzer, S., Bowers, D., Tett, P.B., 2000. Seasonal changes in colour ratios and optically active constituents in the optical Case-2 waters of the Menai Strait, North Wales. Int. J. Remote Sens. 21, 2225–2246.
Lin, M.Y., Lindsay, H.M., Weitz, D.A., Ball, R.C., Klein, R., Meakin, P., 1989. Universality in colloid aggregation. Nature 339, 360–362.
Logan, B.E., Wilkinson, D.B., 1990. Fractal geometry of marine snow and other biological aggregates. Limnol. Oceanogr. 35, 130–136.
Maggi, F., 2007. Variable fractal dimension: a major control for floc structure and flocculation kinematics of suspended cohesive sediment. J. Geophys. Res. 112, C07012. http://dx.doi.org/10.1029/2006JC003951.
Maggi, F., 2013. The settling velocity of mineral, biomineral, and biological particles and aggregates in water. J. Geophys. Res.-Oceans 218, 2118–2132. http://dx.doi.org/10.1002/jgrc.20086.
Mikkelsen, O.A., Hill, P.S., Milligan, T.G., 2006. Single-grain, microfloc and macrofloc volume variations observed with a LISST-100 and a digital floc camera. J. Sea Res. 55, 87–102.
Neukermans, G., Loisel, H., Meriaux, X., Astoreca, R., McKee, D., 2012. In situ variability of mass-specific beam attenuation and backscattering of marine particles with respect to particle size, density, and composition. Limnol. Oceanogr. 57, 124–144.
Orbach, R., 1986. Dynamics of fractal networks. Science 231, 814–819.
Pak, H., Zaneveld, J.R.V., 1977. Bottom nepheloid layers and bottom mixed layers observed on the continental shelf off Oregon. J. Geophys. Res.-Oceans Atmos. 82, 3921–3931.
Pak, H., Zaneveld, J.R.V., Kitchen, J., 1980. Intermediate nepheloid layers observed off Oregon and Washington. J. Geophys. Res.-Oceans Atmos. 85, 6697–6708.
Pak, H., Zaneveld, J.R.V., Spinrad, R.W., 1984. Vertical distribution of suspended particulate matter in the Zaire River, estuary and plume. Neth. J. Sea Res. 17, 412–425.
Peng, F., Effler, S.W., 2007. Suspended minerogenic particles in a reservoir: light-scattering features from individual particle analysis. Limnol. Oceanogr. 52, 204–216.
Plank, W.S., Ronald, J., Pak, H., Zaneveld, V., 1973. Distribution of suspended matter in Panama Basin. J. Geophys. Res. 78, 7113–7121.
Reynolds, R.A., Stramski, D., Wright, V.M., Wozniak, S.B., 2010. Measurements and characterization of particle size distributions in coastal waters. J. Geophys. Res. 115, C08024. http://dx.doi.org/10.1029/2009JC005930.
Sheldon, R.W., 1972. Size separation of marine seston by membrane and glass-fiber filters. Limnol. Oceanogr. 17 (3), 494–498.
Slade, W.H., Boss, E., Russo, C., 2011. Effects of particle aggregation and disaggregation on their inherent optical properties. Opt. Express 19, 7945–7959.
Spinrad, R.W., Zaneveld, J.R.V., Kitchen, J.C., 1983. A study of the optical characteristics of the suspended particles in the benthic nepheloid layer of the Scotian rise. J. Geophys. Res.-Oceans Atmos. 88, 7641–7645.
Stavn, R.H., Rick, H.J., Falster, A.V., 2009. Correcting the errors from variable sea salt retention and water of hydration in loss on ignition analysis: implications for studies of estuarine and coastal waters. Estuar. Coast. Shelf Sci. 81, 575–582.
Stemmann, L., Boss, E., 2012. Plankton and particle size and packaging: from determining optical properties to driving the biological pump. In: Carlson, C.A., Giovannoni, S.J. (Eds.), Annu. Rev. Mar. Sci. 4, 263–290.
Wiberg, P.L., Drake, D.E., Cacchione, D.A., 1994. Sediment resuspension and bed armoring during high bottom stress events on the northern California inner continental shelf: measurements and predictions. Cont. Shelf Res. 14, 1191–1219.
Wozniak, S.B., Stramski, D., Stramska, M., Reynolds, R.A., Wright, V.M., Miksic, E.Y., Cichocka, M., Cieplak, A.M., 2010. Optical variability of seawater in relation to particle concentration, composition, and size distribution in the nearshore marine environment at Imperial Beach, California. J. Geophys. Res. 115, C08027. http://dx.doi.org/10.1029/2009JC005554.
Zaneveld, R.J.V., Pak, H.J., 1979. Optical and particulate properties at oceanic fronts. J. Geophys. Res.-Oceans Atmos. 84, 7781–7790.